

Boundary Layer Realization in Thin Elastic 3-D Domains and 2-D Hierarchic Plate Models

Monique Dauge[&] and Zohar Yosibash[#]

[&] Institut Mathématique, UMR 6625 du CNRS, Université de Rennes 1,
Campus de Beaulieu, 35042 Rennes, France

[#] Pearlstone Center for Aeronautical Engineering Studies, Mechanical
Engineering Dept., Ben-Gurion University of the Negev, Beer-Sheva, Israel

***Abstract.** Herein we address the behavior of the linear elastic solution in three-dimensional thin domains, especially near the boundaries, and compare it to the approximated solution obtained by dimension reduced 2-D hierarchic plate models. The mathematical analysis is backed-up by numerical simulations using the p -version of the finite element method. We identify mathematically, and more importantly, quantify the engineering quantities which are rapidly changing in a boundary layer. We also investigate how well (if at all) the two-dimensional plate-models solutions approximate the three-dimensional solution inside and outside of the boundary layers.*

1 INTRODUCTION

Plates are viewed in structural engineering practice as three-dimensional components with one of their dimensions, usually denoted by “thickness”, much smaller compared to the other two dimensions. Due to the complexity of a three-dimensional elastic analysis, much attention has been given historically to the derivation of “plate-models”, which can be understood as an application of dimensional reduction principles. These plate models are aimed to approximately solve the three-dimensional problem by a two-dimensional formulation, and the most popular models in engineering practice are the Kirchhoff-Love (K-L) and Reissner-Mindlin (R-M) plate-models. Recently, hierarchic sequence of plate-models were proposed so as to make adaptive selection of the model which is best suited for the purpose of a particular quantity of interest.

The quality of the plate-model must be judged on the basis of how well its exact solution approximates the corresponding three-dimensional problem. Especially, of much interest are the boundary layers which may occur in a three-dimensional plate, and their realization (if possible at all) in plate-models. Although several previous works have addressed the existence of boundary layers in plate-models (especially the R-M model), and

their treatment by the finite-element method, see e.g. [8, 7, 9, 15, 5, 6, 4] and the references therein, none of the previous publications address in details the fully three-dimensional solution and its behavior in the boundary layer. Therefore a comparison of the solution in the boundary layer zone between the three-dimensional domain and two-dimensional models is lacking.

Very recent detailed mathematical analysis on the asymptotics in thin three-dimensional elastic plates [11, 12] makes it possible to identify, and more importantly, quantify the engineering quantities which are rapidly changing in a boundary layer (which is of a magnitude similar to the plate thickness). Furthermore, it is now possible to investigate how well (if at all) the two-dimensional plate-models solutions approximate the three-dimensional solution inside and outside of the boundary layers. To this end, we herein provide explicitly the quantities which exhibit dramatic changes in the boundary layers. We consider the displacements solution in a three-dimensional thin elastic plate of thickness 2ε as an asymptotic inner (in the boundary layer) and outer series of ε . This enables us to investigate and explicitly present which of the engineering quantities are susceptible to radical changes in the boundary layers, and provide visualization of this radical change via numerical experiments as $\varepsilon \rightarrow 0$.

In Section 2 we provide some notations and preliminaries followed by details on the three-dimensional explicit solution in Section 3. The model problems which are considered for numerical visualization of the mathematical analysis are outlined in Section 4. The mathematical results are demonstrated by numerical experimentation for three-dimensional thin domains in Section 5. We then provide a brief summary on two-dimensional hierarchic plate models in Section 6, followed by various two-dimensional hierarchic plate-model solutions which are compared to the three-dimensional solution and the differences in the behavior especially in boundary layers are emphasized in Section 7. These solutions are obtained using the p -version finite element method. We conclude with a summary and conclusions in Section 8.

2 NOTATIONS AND PRELIMINARIES

We denote by \mathbf{u}^ε the displacement field in a thin elastic three-dimensional domain Ω^ε of thickness 2ε .

The domain Ω^ε is defined as follows:

$$\Omega^\varepsilon = \omega \times (-\varepsilon, +\varepsilon), \quad \text{with } \omega \subset \mathbb{R}^2 \text{ a regular domain.}$$

In general, let $\mathbf{u} = (u_1, u_2, u_3)^\top$ denote the displacement field, and let \mathbf{e} denote the associated linearized strain tensor $e_{ij} = \frac{1}{2}(\partial_i u_j + \partial_j u_i)$, where $\partial_i \equiv \partial/\partial x_i$. The stress tensor $\boldsymbol{\sigma}$ is given by Hooke's law

$$\boldsymbol{\sigma} = [A] \mathbf{e},$$

where $[A] = (A_{ijkl})$ is the compliance tensor of an isotropic material expressed in terms of the Lamé constants λ and μ :

$$A_{ijkl} = \lambda \delta_{ij} \delta_{kl} + \mu (\delta_{ik} \delta_{jl} + \delta_{il} \delta_{jk}).$$

In the sequel we will use either the Lamé constants or the equivalent engineering material coefficients:

$$\text{Young modulus } E = \frac{\mu(3\lambda + 2\mu)}{\lambda + \mu} \quad \text{and Poisson ratio } \nu = \frac{\lambda}{2(\lambda + \mu)}.$$

The inward traction field on a point of the boundary is $\mathbf{T} = (T_1, T_2, T_3)^\top$ defined as $\boldsymbol{\sigma} \cdot \mathbf{n}$ where \mathbf{n} is the unit interior normal to the boundary.

For simplicity of presentation it is assumed that the boundary conditions on the upper and lower faces of the plate, i.e. $x_3 = \pm\varepsilon$, are traction free, and on the lateral faces

$$\partial\Omega_L^\varepsilon = \partial\omega \times (-\varepsilon, +\varepsilon),$$

one of the eight possible combinations of homogeneous boundary conditions denoted by $\textcircled{\mathbf{i}}$ where $\mathbf{i} = 1, \dots, 8$ are prescribed. The eight different lateral boundary conditions are combinations of three homogeneous displacements or tractions: normal, horizontal tangential and vertical.

To \mathbf{u} we associate its horizontal tangential component $u_s := u_1n_2 - u_2n_1$ and its normal component $u_n := \mathbf{u} \cdot \mathbf{n} = u_1n_1 + u_2n_2$ on $\partial\Omega_L^\varepsilon$, the vertical component being u_3 and similar notations apply to \mathbf{T} . To each boundary condition $\textcircled{\mathbf{i}}$ corresponds two complementary sets of indices $A_{\textcircled{\mathbf{i}}}$ and $B_{\textcircled{\mathbf{i}}}$ where $A_{\textcircled{\mathbf{i}}}$ is attached to the Dirichlet conditions of $\textcircled{\mathbf{i}}$, i.e. $u_a = 0$ for each index $a \in A_{\textcircled{\mathbf{i}}}$. The Neumann conditions are $T_b = 0$ for each index $b \in B_{\textcircled{\mathbf{i}}}$. Here is the table of the eight possible lateral boundary conditions.

Table 1: *The eight possible lateral homogeneous boundary conditions and their engineering notation*

$\textcircled{\mathbf{i}}$	Type	Dirichlet	Neumann	$A_{\textcircled{\mathbf{i}}}$	$B_{\textcircled{\mathbf{i}}}$
$\textcircled{1}$	hard clamped	$\mathbf{u} = 0,$		$\{s, n, 3\}$	
$\textcircled{2}$	soft clamped	$u_n, u_3 = 0,$	$T_s = 0$	$\{n, 3\}$	$\{s\}$
$\textcircled{3}$	hard simply supported	$u_s, u_3 = 0,$	$T_n = 0$	$\{s, 3\}$	$\{n\}$
$\textcircled{4}$	soft simply supported	$u_3 = 0,$	$T_n, T_s = 0$	$\{3\}$	$\{s, n\}$
$\textcircled{5}$	frictional I	$u_s, u_n = 0,$	$T_3 = 0$	$\{s, n\}$	$\{3\}$
$\textcircled{6}$	sliding edge	$u_n = 0,$	$T_s, T_3 = 0$	$\{n\}$	$\{s, 3\}$
$\textcircled{7}$	frictional II	$u_s = 0,$	$T_n, T_3 = 0$	$\{s\}$	$\{n, 3\}$
$\textcircled{8}$	free		$\mathbf{T} = 0$		$\{s, n, 3\}$

To each boundary condition $\textcircled{\mathbf{i}}$ we associate a space of kinematically admissible displacements:

$$V_{\textcircled{\mathbf{i}}}(\Omega^\varepsilon) = \left\{ \mathbf{v} \in [H^1(\Omega^\varepsilon)]^3 ; \quad v_a = 0 \text{ on } \partial\Omega_L^\varepsilon \quad \forall a \in A_{\textcircled{\mathbf{i}}} \right\}.$$

Then, the weak formulation of the elasticity problem in the three-dimensional domain is stated:

$$\left\{ \begin{array}{l} \text{Seek } \mathbf{u}^\varepsilon \in V_{\textcircled{\mathbf{i}}}(\Omega^\varepsilon), \text{ such that} \\ \int_{\Omega^\varepsilon} A e(\mathbf{u}^\varepsilon) : e(\mathbf{v}) = \int_{\Omega^\varepsilon} \mathbf{f}^\varepsilon \cdot \mathbf{v}, \quad \forall \mathbf{v} \in V_{\textcircled{\mathbf{i}}}(\Omega^\varepsilon), \end{array} \right. \quad (2.1)$$

where \mathbf{f}^ε represents the volume distributed force.

Noting by Greek index α the values in $\{1, 2\}$ corresponding to the in-plane variables, we can state the strong formulation equivalent to (2.1) of the three-dimensional plate problem in Ω^ε as

$$\begin{aligned} (\lambda + \mu) \partial_\alpha \operatorname{div} \mathbf{u}^\varepsilon + \mu \Delta u_\alpha^\varepsilon &= -f_\alpha^\varepsilon, & \alpha = 1, 2, \\ (\lambda + \mu) \partial_3 \operatorname{div} \mathbf{u}^\varepsilon + \mu \Delta u_3^\varepsilon &= -f_3^\varepsilon. \end{aligned}$$

with traction free boundary conditions on the top and bottom faces of the plate $x_3 = \pm\varepsilon$:

$$\begin{aligned} 2\mu e_{\alpha 3} \mathbf{u}^\varepsilon &= 0, & \alpha = 1, 2, \\ 2\mu \partial_3 u_3^\varepsilon + \lambda \operatorname{div} \mathbf{u}^\varepsilon &= 0. \end{aligned}$$

The boundary conditions on the lateral side $\partial\Omega_L^\varepsilon$ are

$$u_a^\varepsilon = 0, \quad \forall a \in A_{\textcircled{i}} \quad \text{and} \quad T_b^\varepsilon = 0, \quad \forall b \in B_{\textcircled{i}}.$$

To examine the behavior of the engineering quantities of interest as $\varepsilon \rightarrow 0$, we scale the x_3 coordinate by a factor of $1/\varepsilon$, to obtain a standard domain $\Omega = \omega \times (-1, 1)$. Because we are interested in the lateral boundary layers in the neighborhood of $\partial\omega$, we introduce the new scaled parameter $N = n/\varepsilon$, where n is an axis inward and normal to the boundary, and we also define $X_3 = x_3/\varepsilon$, see Figure 1. The curvature radius of $\partial\omega$

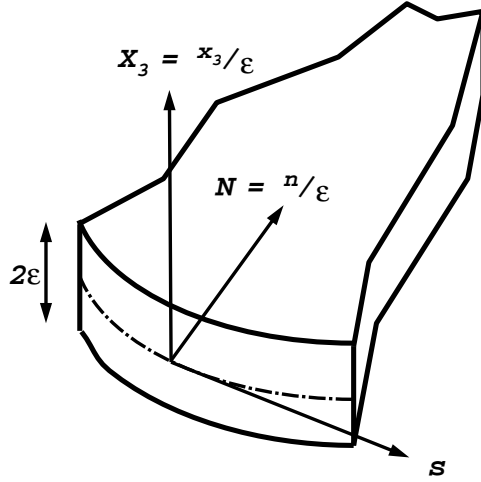


Figure 1: *The coordinate system near plate's lateral boundary.*

inside ω at s is denoted by $R = R(s)$, and we recall that $\frac{1}{R} = \kappa$ is the curvature. Notice that for straight boundaries $\kappa = 0$.

Like in [11, 12], we assume that the body forces behave like fixed profiles in the scaled vertical variable X_3 and that they are of order of ε in the vertical direction, namely

$$f_\alpha^\varepsilon(x) = f_\alpha(x_1, x_2, X_3), \quad \alpha = 1, 2, \quad f_3^\varepsilon(x) = \varepsilon f_3(x_1, x_2, X_3). \quad (2.2)$$

with the data $\mathbf{f} = (f_1, f_2, f_3)^\top$ regular up to the boundary, i.e. $\mathbf{f} \in C^\infty(\bar{\Omega})^3$. These assumptions ensure that the displacements have an asymptotic expansion as $\varepsilon \rightarrow 0$ as discussed in the next section, and that this expansion starts “near” ε^0 . Note that, as we are in the framework of linearized elasticity, by superposition we can construct displacement asymptotics for any body forces in the form $\sum_k \varepsilon^k \mathbf{f}^k(x_1, x_2, X_3)$. Moreover, any force which can be expanded as a series $\sum_k \varepsilon^k \mathbf{g}^k(x_1, x_2, x_3)$ of smooth functions in the unscaled variables (x_1, x_2, x_3) , has also the previous form.

The condensed notation \mathbf{u}_* is used for $(u_1, u_2)^\top$, $\operatorname{div}_* \mathbf{u}_*$ denotes $\partial_1 u_1 + \partial_2 u_2$ and Δ_* denotes the horizontal Laplacian $\partial_{11} + \partial_{22}$.

3 THREE-DIMENSIONAL SOLUTION

The displacements \mathbf{u}^ε in Ω^ε can be split into a bending part \mathbf{u}_b^ε and a membrane (or stretching) part \mathbf{u}_m^ε , cf [13], according to

$$\begin{aligned} \mathbf{u}_{b,\alpha}^\varepsilon(x_3) &= \frac{1}{2}(\mathbf{u}_\alpha^\varepsilon(x_3) - \mathbf{u}_\alpha^\varepsilon(-x_3)), \quad \alpha = 1, 2, & \mathbf{u}_{b,3}^\varepsilon(x_3) &= \frac{1}{2}(\mathbf{u}_3^\varepsilon(x_3) + \mathbf{u}_3^\varepsilon(-x_3)) \\ \mathbf{u}_{m,\alpha}^\varepsilon(x_3) &= \frac{1}{2}(\mathbf{u}_\alpha^\varepsilon(x_3) + \mathbf{u}_\alpha^\varepsilon(-x_3)), \quad \alpha = 1, 2, & \mathbf{u}_{m,3}^\varepsilon(x_3) &= \frac{1}{2}(\mathbf{u}_3^\varepsilon(x_3) - \mathbf{u}_3^\varepsilon(-x_3)). \end{aligned}$$

Thus the in-plane components of \mathbf{u}_b^ε are odd with respect to x_3 and its vertical component is even, whereas the in-plane components of \mathbf{u}_m^ε are even and its vertical component is odd. Of course, \mathbf{u}_b^ε is the solution of (2.1) corresponding to the bending part of the body forces \mathbf{f}_b^ε , and similarly for the membrane.

3.1 Full expansion of displacements

The bending and membrane parts of the displacement \mathbf{u}^ε solution of (2.1) can be expanded in the following way in the sense of asymptotic expansions*

$$\mathbf{u}_b^\varepsilon \simeq \frac{1}{\varepsilon} \mathbf{u}_{\text{KL},b}^0 + \mathbf{u}_{\text{KL},b}^1 + \varepsilon(\mathbf{u}_{\text{KL},b}^2 + \mathbf{v}_b^1 + \boldsymbol{\varphi}_b^1) + \cdots + \varepsilon^k(\mathbf{u}_{\text{KL},b}^{k+1} + \mathbf{v}_b^k + \boldsymbol{\varphi}_b^k) \cdots \quad (3.1)$$

$$\mathbf{u}_m^\varepsilon \simeq \mathbf{u}_{\text{KL},m}^0 + \varepsilon(\mathbf{u}_{\text{KL},m}^1 + \mathbf{v}_m^1 + \boldsymbol{\varphi}_m^1) + \cdots + \varepsilon^k(\mathbf{u}_{\text{KL},m}^k + \mathbf{v}_m^k + \boldsymbol{\varphi}_m^k) \cdots \quad (3.2)$$

where

- the $\mathbf{u}_{\text{KL},b}^k$ and $\mathbf{u}_{\text{KL},m}^k$ are bending and membrane parts of Kirchhoff-Love displacements and are given as:

$$\mathbf{u}_{\text{KL},b}^k = (-x_3 \partial_1 \zeta_3^k, -x_3 \partial_2 \zeta_3^k, \zeta_3^k)^\top \quad \text{and} \quad \mathbf{u}_{\text{KL},m}^k = (\zeta_1^k, \zeta_2^k, 0)^\top, \quad (3.3)$$

where ζ_1^k , ζ_2^k and ζ_3^k are functions of the in-plane variables x_* and are denoted by “generators” because all terms in (3.1)-(3.2) can be generated by ζ^k .

- The first two terms $\mathbf{u}_{\text{KL},b}^0$ and $\mathbf{u}_{\text{KL},m}^0$ are the well-known limit Kirchhoff-Love displacement vectors [10].

* This means that the difference between the solution of (2.1) and the truncated series of (3.1)-(3.2) at the order k is estimated by $c_k \varepsilon^{k+1}$, cf more precisely [11, 12].

- The $\mathcal{O}(1)$ term $\mathbf{u}_{\text{KL},\text{b}}^1$ manifests the boundary layer profile “pollution” inside the plate, i.e. away from the boundary.
- the \mathbf{v}_{b}^k and \mathbf{v}_{m}^k are bending and membrane parts of a displacement $\mathbf{v}^k = \mathbf{v}^k(x_*, X_3)$ with zero mean value:

$$\forall x_* \in \bar{\omega}, \int_{-1}^{+1} \mathbf{v}^k(x_*, X_3) dX_3 = 0.$$

It is important to notice that \mathbf{v}^k does not depend on ε ;

- the φ_{b}^k and φ_{m}^k are bending and membrane parts of a bounded boundary layer profile $\varphi^k = \varphi^k(s, N, X_3)$ exponentially decreasing as $N \rightarrow \infty$.

We give more information about these different terms.

(i) THE KIRCHHOFF-LOVE DISPLACEMENTS.

$\mathbf{u}_{\text{KL},\text{m}}^k$ and $\mathbf{u}_{\text{KL},\text{b}}^k$ are determined by three functions defined on ω : $(\zeta_1^k, \zeta_2^k)^\top = \zeta_*^k$ and ζ_3^k , respectively. The in-plane displacement ζ_*^k is solution of the “membrane equation”:

$$\mu [\Delta_*] \zeta_*^k + (\tilde{\lambda} + \mu) \nabla_* \operatorname{div}_* \zeta_*^k = \mathbf{R}_{\text{m}}^k, \quad (3.4)$$

whereas ζ_3^k solves the “bending equation”:

$$(\tilde{\lambda} + 2\mu) \Delta_*^2 \zeta_3^k = R_{\text{b}}^k, \quad (3.5)$$

with $\tilde{\lambda} = 2\lambda\mu(\lambda + 2\mu)^{-1}$ and $[\Delta_*]$ the vectorial horizontal Laplacian. The right hand side of (3.4) for ζ_*^0 is given by:

$$\mathbf{R}_{\text{m}}^0(x_*) = -\frac{1}{2} \int_{-1}^{+1} \mathbf{f}_*(x_*, X_3) dX_3$$

and the right hand side of (3.5), for ζ_3^0 is:

$$R_{\text{b}}^0(x_*) = \frac{3}{2} \left[\int_{-1}^{+1} f_3 dX_3 + \operatorname{div}_* \left(\int_{-1}^{+1} X_3 \mathbf{f}_* dX_3 \right) \right]$$

and for ζ^k , $k = 1, 2, \dots$ the right hand sides are provided in Table 6 in [11, Part I] or Table 5 in [11, Part II].

The type of boundary conditions on $\partial\omega$ for the generators are provided in Tables 2 & 3 in [11, Part I & II], and we only remark several interesting properties:

- For the four cases ①, ②, ③, and ④, (unlike the other four cases) the boundary conditions for the partial differential equations involving ζ^0 are all 0.
- The boundary conditions for ζ^1 are special traces of ζ^0 according to Table 3 in [11, Part I & II]. It is important to note that the boundary conditions consist of traces associated with the boundary layer profiles, hence, the boundary layers influence ζ^1 through these boundary conditions.
- For the four cases ⑤, ⑥, ⑦, and ⑧, $\zeta_1^1 = \zeta_2^1 = 0$.

(ii) THE FIRST DISPLACEMENTS \mathbf{v}^1 .

The displacement vectors \mathbf{v}_b^1 and \mathbf{v}_m^1 are also completely determined by ζ^0 , and their expressions are given by:

$$\mathbf{v}_b^1(x_*, X_3) = \frac{\nu}{6(1-\nu)} \left(0, 0, (3X_3^2 - 1) \Delta_* \zeta_3^0 \right)^\top, \quad (3.6)$$

$$\mathbf{v}_m^1(x_*, X_3) = \frac{\nu}{6(1-\nu)} \left(0, 0, -6X_3 \operatorname{div}_* \zeta_*^0 \right)^\top. \quad (3.7)$$

(iii) THE BOUNDARY LAYER FIRST PROFILES FOR CASES ①, ②, ③, AND ④.

φ_b^1 can be described as a sum of two terms in tensor product form in the variables s and (N, X_3) :

$$\varphi_b^1 = a(s) \varphi_b^{1a}(N, X_3) + b(s) \varphi_b^{1b}(N, X_3), \quad (3.8)$$

whereas φ_m^1 has an expression in tensor product form

$$\varphi_m^1 = c(s) \varphi_m^{1c}(N, X_3). \quad (3.9)$$

Here φ_b^{1a} , φ_b^{1b} and φ_m^{1c} are typical profiles whose components in the horizontal tangent, normal and vertical directions have special behaviors with respect to X_3 :

$$\begin{aligned} \varphi_b^{1a} &= (0, \text{odd}, \text{even})^\top \\ \varphi_b^{1b} &= (\text{odd}, 0, 0)^\top \\ \varphi_m^{1c} &= (0, \text{even}, \text{odd})^\top. \end{aligned}$$

The functions a, b, c are given as traces of ζ^0 along the boundary $\partial\omega$ according to the following:

Table 2a: Values of $a(s)$, $b(s)$ and $c(s)$ for ① - ④ BCs.

Case	$a(s)$	$b(s)$	$c(s)$
① and ②	$\Delta_* \zeta_3^0$	0	$\operatorname{div}_* \zeta_*^0$
③	$\kappa \partial_n \zeta_3^0$	0	$\kappa \zeta_n^0$
④	$\kappa \partial_n \zeta_3^0$	$\partial_s (\partial_n \zeta_3^0)$	$\operatorname{div}_* \zeta_*^0$

Note the presence of κ in front of the traces for the hard simple support case: the existence of boundary layer terms is linked to non zero curvature.

(iv) THE BOUNDARY LAYER FIRST PROFILE FOR CASES ⑤, ⑥, ⑦, AND ⑧.

In contrast to the previous four “clamped” lateral boundary conditions, the normal and transverse components of φ^1 are zero, i.e. $\varphi_N^1 = \varphi_3^1 = 0$, and the only nonzero component is $\varphi_{b,s}^1$. Moreover, $\varphi_m^1 = 0$. φ_b^1 is still given by (3.8), with $a(s) = 0$ and $b(s)$ is given according to the following Table:

Table 2b: Values of $b(s)$ for ⑤ - ⑧ BCs.

Case	$b(s)$
⑤	$\partial_s \zeta_3^0$
⑥	$\kappa \partial_s \zeta_3^0$
⑦	$\partial_s \zeta_3^0$
⑧	$(\partial_n + \kappa) \partial_s \zeta_3^0$

(v) THE RELATION BETWEEN CURVATURE AND BOUNDARY LAYER FIRST PROFILES.

There are boundary conditions for which boundary layers do not develop in case the boundary is straight. These are ③ and ⑥. Boundary layers always develop for curved boundaries. A summary of the cases at which boundary layers do appear is given in Table 3. The letters s, N, X_3 denote if boundary layers are in the horizontal tangential, normal or vertical component of the displacement fields.

Table 3: Existence of boundary layers for the eight possible lateral homogeneous boundary conditions.

① Type	Straight Boundary	Curved Boundary
① hard clamped	N, X_3	N, X_3
② soft clamped	N, X_3	N, X_3
③ hard simply supported	—	N, X_3
④ soft simply supported	s, N, X_3	s, N, X_3
⑤ frictional I	s	s
⑥ sliding edge	—	s
⑦ frictional II	s	s
⑧ free	s	s

3.2 First terms of Displacements

To realize the specific quantities which play a significant role in each of the various zones in the thin plate we present herein the first terms in the expansion (3.1)-(3.2), up to $\mathcal{O}(\varepsilon^2)$. Throughout the plate $x_3/\varepsilon \equiv X_3$, see Figure 1.

To visualize which of the values approach zero as $\varepsilon \rightarrow 0$, we express these in terms of the $\mathcal{O}(1)$ variables s, N, X_3 used in the boundary layer and x_1, x_2, X_3 used elsewhere. With this in mind, (3.1)-(3.2) take the form:

$$\mathbf{u}_b^\varepsilon = \begin{pmatrix} -X_3 \partial_1 \zeta_3^0 & -\varepsilon X_3 \partial_1 \zeta_3^1 & +0 & +0 \\ -X_3 \partial_2 \zeta_3^0 & -\varepsilon X_3 \partial_2 \zeta_3^1 & +0 & +0 \\ \frac{1}{\varepsilon} \zeta_3^0 & +\zeta_3^1 & +\varepsilon \zeta_3^2 & +\varepsilon v_{b,3}^1 \end{pmatrix} + \varepsilon \boldsymbol{\varphi}_b^1 + \mathcal{O}(\varepsilon^2) \quad (3.10)$$

$$\mathbf{u}_m^\varepsilon = \begin{pmatrix} \zeta_1^0 & +\varepsilon\zeta_1^1 & +0 \\ \zeta_2^0 & +\varepsilon\zeta_2^1 & +0 \\ 0 & +0 & +\varepsilon v_{m,3}^1 \end{pmatrix} + \varepsilon \boldsymbol{\varphi}_m^1 + \mathcal{O}(\varepsilon^2) \quad (3.11)$$

where the symbol $\mathcal{O}(\varepsilon^2)$ means that the remainder is uniformly bounded by $c\varepsilon^2$ and $\boldsymbol{\varphi}^1$ is determined according to the eight canonical cases in (3.8)-(3.9).

Examining (3.10)-(3.11) it may be noticed that the displacement field is dominated by the Kirchhoff-Love components, and especially the vertical bending component of $\mathbf{u}_{\text{KL},b}^0$ is much larger than any other displacement component (this is commonly known). However, in order to visualize the boundary layer effects in the bending displacement field, we filter out constants in X_3 by the introduction of the quantities, defined in the neighborhood of ω 's boundary:

$$\begin{aligned} J_i[\mathbf{u}](s, N) &= \frac{1}{\varepsilon} \int_{-\varepsilon}^{\varepsilon} \frac{u_3(s, N, X_3)}{\varepsilon} P_i\left(\frac{x_3}{\varepsilon}\right) dx_3 \\ &= \frac{1}{\varepsilon} \int_{-1}^{+1} u_3(s, N, X_3) P_i(X_3) dX_3, \quad i = 2, 4, 6 \end{aligned} \quad (3.12)$$

where $P_i(t)$ is the Legendre polynomial of order i . Because ζ_3^0 , ζ_3^1 and ζ_3^2 are constants in respect to x_3 , then they are orthogonal to P_i ($i \neq 0$). Computing $J_i[\mathbf{u}](s, N)$ at a given point s of the boundary along the inward normal $0 \leq n/2\varepsilon \leq 1$ emphasizes the boundary layers in the displacements fields. Since $v_{b,3}^1$ has a term which depends on X_3^2 , see (3.6), then we expect that $J_2[\mathbf{u}](s, N)$ will vary in the boundary layer zone due to the effect of the boundary layer profile, but will become constant outside of the boundary layer. This will be demonstrated numerically in Section 5.

3.3 First terms of Strains

A more pronounced influence of the boundary layers shows up when examining the strain components. We herein denote the bending and membrane strain vectors associated with \mathbf{u}_b and \mathbf{u}_m respectively, by

$$\mathbf{e}_b = (e_{b,11} \ e_{b,22} \ e_{b,33} \ e_{b,23} \ e_{b,13} \ e_{b,12})^\top \quad \text{and} \quad \mathbf{e}_m = (e_{m,11} \ e_{m,22} \ e_{m,33} \ e_{m,23} \ e_{m,13} \ e_{m,12})^\top.$$

We investigate the strain asymptotics successively outside and inside the boundary layer zone.

(i) OUTSIDE THE BOUNDARY LAYER ZONE.

In a region of the form $\omega_0 \times (-\varepsilon, \varepsilon)$ where $\bar{\omega}_0 \subset \omega$, the effect of the boundary layer terms is not visible since the $\boldsymbol{\varphi}^k$ are exponentially decreasing. Then the asymptotics of \mathbf{e}_b and \mathbf{e}_m contains only the terms coming from $\mathbf{u}_{\text{KL},b}^k$, \mathbf{v}_b^k and $\mathbf{u}_{\text{KL},m}^k$, \mathbf{v}_m^k respectively, namely

$$\begin{pmatrix} e_{b,11} \\ e_{b,22} \\ e_{b,33} \\ e_{b,23} \\ e_{b,13} \\ e_{b,12} \end{pmatrix} = \begin{pmatrix} -X_3 \partial_{11} \zeta_3^0 & -\varepsilon X_3 \partial_{11} \zeta_3^1 & +0 \\ -X_3 \partial_{22} \zeta_3^0 & -\varepsilon X_3 \partial_{22} \zeta_3^1 & +0 \\ 0 & +0 & +\frac{\nu}{1-\nu} X_3 \Delta_* \zeta_3^0 \\ 0 & +0 & +\varepsilon \frac{\nu}{6(1-\nu)} (3X_3^2 - 1) \partial_2 \Delta_* \zeta_3^0 \\ 0 & +0 & +\varepsilon \frac{\nu}{6(1-\nu)} (3X_3^2 - 1) \partial_1 \Delta_* \zeta_3^0 \\ -X_3 \partial_{12} \zeta_3^0 & -\varepsilon X_3 \partial_{12} \zeta_3^1 & +0 \end{pmatrix} + \dots$$

$$= \begin{pmatrix} -X_3 \partial_{11} \zeta_3^0 \\ -X_3 \partial_{22} \zeta_3^0 \\ \frac{\nu}{1-\nu} X_3 \Delta_* \zeta_3^0 \\ 0 \\ 0 \\ -X_3 \partial_{12} \zeta_3^0 \end{pmatrix} + \mathcal{O}(\varepsilon) \quad (3.13)$$

and

$$\begin{pmatrix} e_{m,11} \\ e_{m,22} \\ e_{m,33} \\ e_{m,23} \\ e_{m,13} \\ e_{m,12} \end{pmatrix} = \begin{pmatrix} \partial_1 \zeta_1^0 & + \varepsilon \partial_1 \zeta_1^1 & + 0 \\ \partial_2 \zeta_2^0 & + \varepsilon \partial_2 \zeta_2^1 & + 0 \\ 0 & + 0 & -\frac{\nu}{1-\nu} \operatorname{div}_* \zeta_*^0 \\ 0 & + 0 & -\varepsilon \frac{\nu}{2(1-\nu)} X_3 \partial_2 \operatorname{div}_* \zeta_*^0 \\ 0 & + 0 & -\varepsilon \frac{\nu}{2(1-\nu)} X_3 \partial_1 \operatorname{div}_* \zeta_*^0 \\ \frac{1}{2}(\partial_2 \zeta_1^0 + \partial_1 \zeta_2^0) & + \varepsilon \frac{1}{2}(\partial_2 \zeta_1^1 + \partial_1 \zeta_2^1) & + 0 \end{pmatrix} + \dots$$

$$= \begin{pmatrix} \partial_1 \zeta_1^0 \\ \partial_2 \zeta_2^0 \\ -\frac{\nu}{1-\nu} \operatorname{div}_* \zeta_*^0 \\ 0 \\ 0 \\ \frac{1}{2}(\partial_2 \zeta_1^0 + \partial_1 \zeta_2^0) \end{pmatrix} + \mathcal{O}(\varepsilon) \quad (3.14)$$

Thus we can see that, outside the boundary layer zone, the components e_{23} and e_{13} are of order ε , unlike the four other ones in general.

(ii) INSIDE THE BOUNDARY LAYER ZONE.

For this reason, we investigate more specially the two components e_{12} and e_{13} inside the boundary layer zone in order to make the boundary layer visible. Now, instead of the cartesian in-plane components, it is more natural to consider the tangential and normal components, namely for the strains

$$e_{s3} = \frac{1}{2}(\partial_s u_3 + \partial_3 u_s) \quad \text{and} \quad e_{n3} = \frac{1}{2}(\partial_n u_3 + \partial_3 u_n).$$

For ①, ② and ③:

$$\begin{pmatrix} e_{b,s3} \\ e_{b,n3} \end{pmatrix} = \begin{pmatrix} 0 \\ \frac{1}{2}(\partial_{X_3} \varphi_{b,N}^1 + \partial_N \varphi_{b,3}^1) \end{pmatrix} + \frac{\varepsilon}{2} \begin{pmatrix} \partial_s v_{b,3}^1 \\ \partial_n v_{b,3}^1 \end{pmatrix} + \mathcal{O}(\varepsilon^2) \quad (3.15)$$

and

$$\begin{pmatrix} e_{m,s3} \\ e_{m,n3} \end{pmatrix} = \begin{pmatrix} 0 \\ \frac{1}{2}(\partial_{X_3} \varphi_{m,N}^1 + \partial_N \varphi_{m,3}^1) \end{pmatrix} + \frac{\varepsilon}{2} \begin{pmatrix} \partial_s v_{m,3}^1 \\ \partial_n v_{m,3}^1 \end{pmatrix} + \mathcal{O}(\varepsilon^2). \quad (3.16)$$

Thus the strain component e_{n3} is influenced mainly by the boundary layer term which is of order 1, and influenced at the order ε by the v^1 term.

For condition ④, we still have (3.16), but instead of (3.15), due to the presence of the new bending tangential component $\varphi_{b,s}^{1b}$ in the boundary layer terms, we have now:

$$\begin{pmatrix} e_{b,s3} \\ e_{b,n3} \end{pmatrix} = \begin{pmatrix} \frac{1}{2} \partial_s \partial_n \zeta_3^0(s) \partial_{X_3} \varphi_{b,s}^{1b} \\ \frac{1}{2} \kappa \partial_n \zeta_3^0(s) (\partial_{X_3} \varphi_{b,N}^{1a} + \partial_N \varphi_{b,3}^{1a}) \end{pmatrix} + \frac{\varepsilon}{2} \begin{pmatrix} \partial_s v_{b,3}^1 \\ \partial_n v_{b,3}^1 \end{pmatrix} + \mathcal{O}(\varepsilon^2). \quad (3.17)$$

Thus e_{n3} in the boundary layer zone is of order ε for straight boundaries but of order 1 for curved boundaries.

For boundary conditions ⑤ - ⑧, since $\varphi_m^1 \equiv 0$, only the bending part is of interest:

$$\begin{pmatrix} e_{b,s3} \\ e_{b,n3} \end{pmatrix} = \begin{pmatrix} \frac{1}{2} \partial_{X_3} \varphi_{b,s}^1 \\ 0 \end{pmatrix} + \frac{\varepsilon}{2} \begin{pmatrix} \partial_s v_{b,3}^1 \\ \partial_n v_{b,3}^1 \end{pmatrix} + \mathcal{O}(\varepsilon^2). \quad (3.18)$$

Here, the strain component e_{s3} is influenced by the boundary layer term at the order 1, and influenced at the order ε by the v^1 term.

4 MODEL PROBLEMS USED FOR DEMONSTRATION PURPOSES

The theoretical results are visualized by computing functionals associated with the boundary layer terms for the different boundary conditions. We consider two configurations: the first one is a rectangular plate, thus with straight edges, whereas the second one is a circular plate, thus the boundary has a non-zero curvature.

(i) RECTANGULAR PLATE.

Its dimensions are $4 \times 1 \times 2\varepsilon$ and it is subjected to a *bending* volume force $\mathbf{f}^\varepsilon = (0, 0, 2\varepsilon)^\top$, see Figure 2. The material properties are: Poisson ratio $\nu = 1/8$ and Young

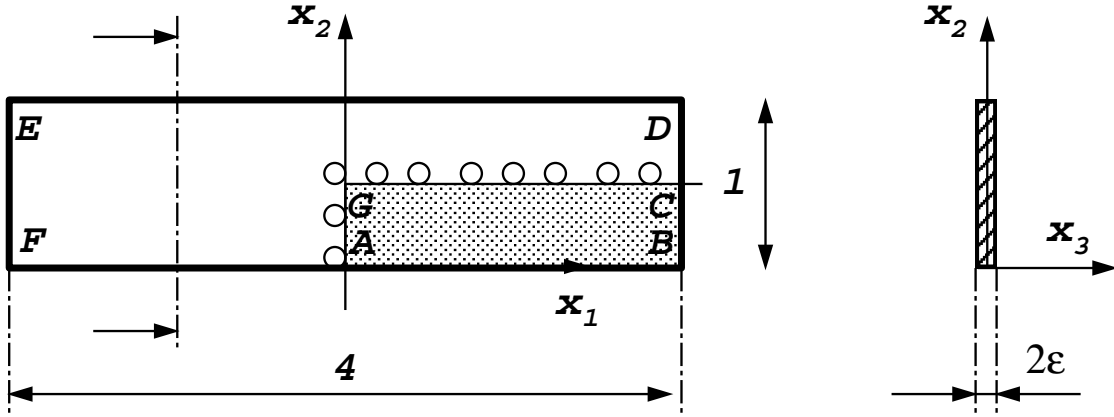


Figure 2: Rectangular plate under consideration.

modulus $E = 27/4$. Being interested in the boundary layers along edge FB of the plate, we keep the other boundaries EF and DB hard clamped, while on the boundaries FB and ED we apply the various eight homogeneous boundary conditions. These boundary conditions give rise to two axes of symmetry, so that only a quarter of the plate may be analyzed, namely plate $ABCG$, with symmetry boundary conditions ⑥ on AG and GC .

We consider a part of this plate which has one of its boundaries along the x_1 axis, so that in the boundary layer zone $x_1 \equiv s$, and $x_2/\varepsilon \equiv N$. Thus, in the neighborhood of the point A , $\partial_1 \equiv \partial/\partial s$, $\partial_2 \equiv \frac{1}{\varepsilon} \partial/\partial N$, and overall the domain $\partial_3 \equiv \frac{1}{\varepsilon} \partial/\partial X_3$.

To visualize the boundary layer influence we compute the normalized root mean square (N-RMS) norm I_{13}^{bl} of $e_{13} = e_{s3}$ and I_{23}^{bl} of $e_{23} = e_{n3}$ inside the boundary layer zone according to the formula

$$I_{\alpha 3}^{bl} = \sqrt{\frac{1}{V} \int_{x_1=0}^1 \int_{x_2=0}^{2\varepsilon} \int_{x_3=-\varepsilon}^{\varepsilon} |e_{\alpha 3}|^2 dV}, \quad \alpha = 1, 2, \quad (4.1)$$

and the N-RMS norm of I_{13}^{out} of e_{13} and I_{23}^{out} of e_{23} away from the boundary layer:

$$I_{\alpha 3}^{out} = \sqrt{\frac{1}{V} \int_{x_1=0}^1 \int_{x_2=0.25}^{0.5} \int_{x_3=-\varepsilon}^{\varepsilon} |e_{\alpha 3}|^2 dV}, \quad \alpha = 1, 2, \quad (4.2)$$

where V denotes the volume of the “box” in which the strain components are sought. *The main interest of this N-RMS norm is that it has the same behavior in ε as the corresponding strain component.*

(ii) CIRCULAR PLATE.

The second configuration under investigation is a circular plate of radius 1 and thickness 2ε as shown in Figure 3. Material properties and volume force remain unchanged. For this

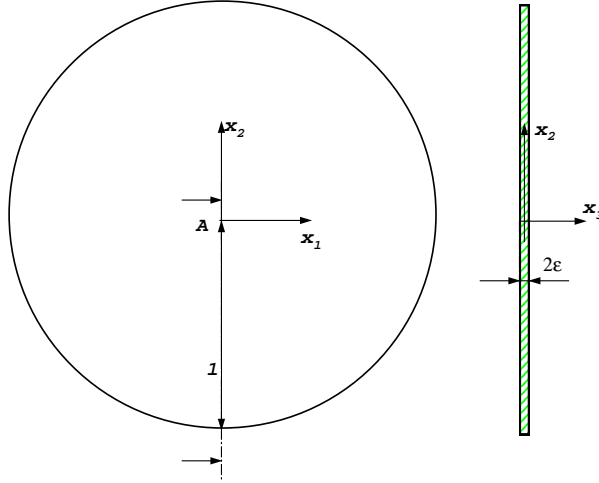


Figure 3: Circular plate under consideration.

case (of a circular boundary) we define

$$I_{n3}^{bl} = \sqrt{\frac{1}{V} \int_{r=1-2\varepsilon}^1 \int_{\theta=0}^{2\pi} \int_{x_3=-\varepsilon}^{\varepsilon} |e_{n3}|^2 r dr d\theta dx_3}, \quad (4.3)$$

where V is the volume of the annulus zone $r \in (1 - 2\varepsilon, 1)$ under consideration.

5 NUMERICAL TESTS FOR THREE-DIMENSIONAL PROBLEMS

In this section numerical results are provided which demonstrate the solution characteristics inside and outside of the boundary layers in three-dimensional domains.

5.1 Visualization of Boundary Layers in a 3-D rectangular plate

A three dimensional p -version finite element model is constructed having two elements in the thickness direction, four elements in the x_2 direction and six elements in the x_1 direction. In the neighborhood of the edges, the mesh is graded so that there are two elements of dimension ε each. See Figure 4 for a typical mesh for $2\varepsilon = 0.1$ and Figure 5 for $2\varepsilon = 0.001$ and ① boundary conditions. The finite element model is constructed

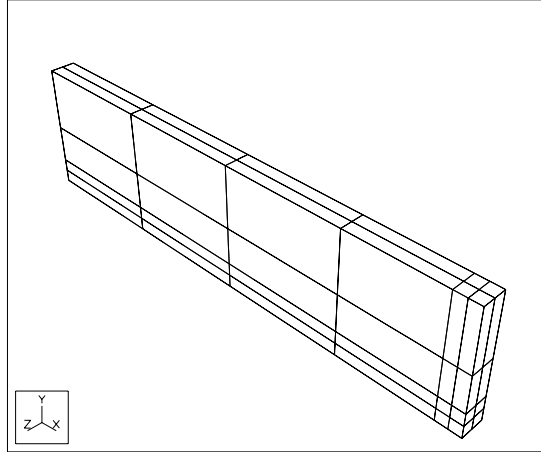


Figure 4: Finite element mesh for the plate with $2\varepsilon = 0.1$.

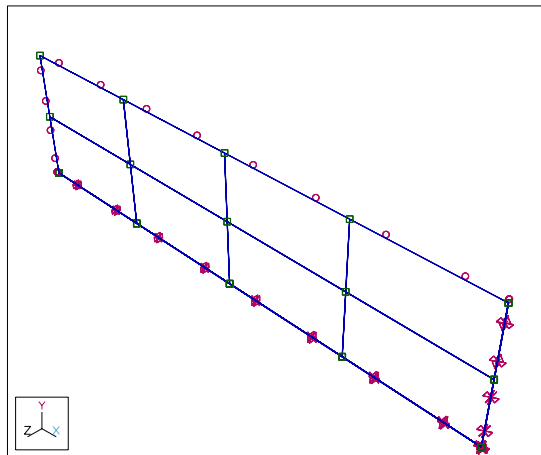


Figure 5: Finite element mesh and boundary conditions for the plate with $2\varepsilon = 0.001$.

parametrically so that the value of 2ε may vary, and we change it from $0.1 (= 10^{-1})$ to $0.00031622777 (= 10^{-3.5})$. Although not visible on Figure 5, there are two elements across the thickness and two elements each of dimension ε in the neighborhood of the boundary. The p -level over each element has been increased from 1 to 8 and the trunk space has been used (see [17]). There are 12,568 degrees of freedom at $p = 8$. An advantage of using p -version finite element methods is this possibility of having “needle

elements” in the boundary layer zone with aspect ratios as large as 10,000 without significant degradation in the numerical performance.

The convergence rate in energy norm for $2\varepsilon = 0.001$ is provided in Figure 6 as a typical example. An *exponential convergence rate* is obtained without thickness-locking phenomenon visible (due to the use of high-order elements). The convergence of the computed data has been examined as well for increasing p -levels in order to evaluate the reliability of the numerical results.

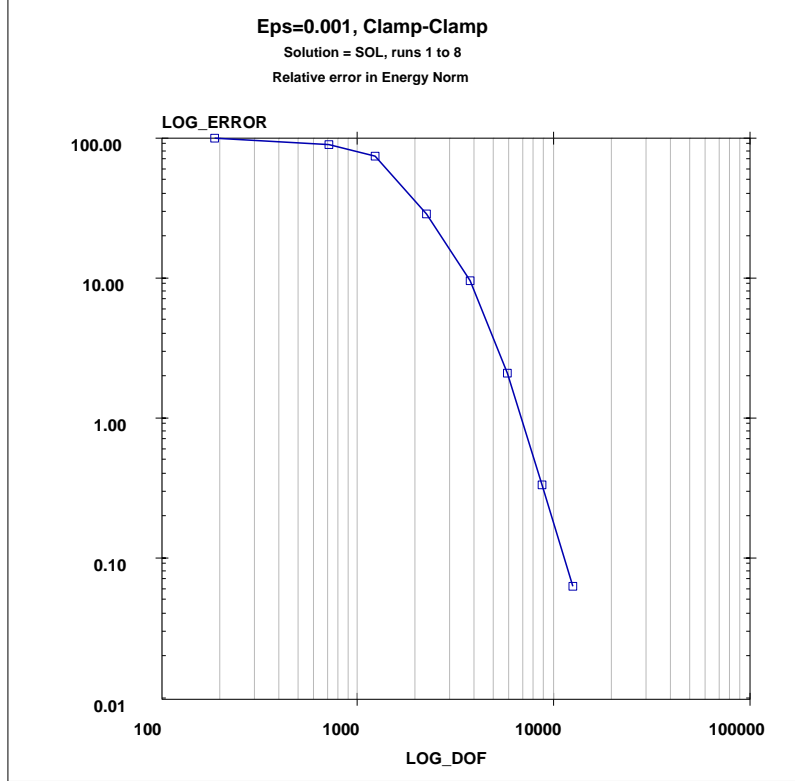


Figure 6: Convergence rate in energy norm, $\textcircled{1}$ BCs, with $2\varepsilon = 0.001$.

(i) BOUNDARY LAYERS IN VERTICAL DISPLACEMENT.

The value of $J_2[\mathbf{u}]$, $J_4[\mathbf{u}]$ and $J_6[\mathbf{u}]$, as defined in (3.12) is computed at a set of equidistant points $(s, N) = (x_1, x_2/2\varepsilon)$ along the line $x_1 = 1$, $0 \leq x_2/2\varepsilon \leq 2$ for clamped boundary conditions $\textcircled{1}$ and shown in Figure 7. The graphs clearly present the existence of the boundary layer profile in the vertical displacement component in three-dimensional domain in the vicinity of the boundary where $x_2/2\varepsilon < 1$. As expected, $J_4[\mathbf{u}] \rightarrow 0$ and $J_6[\mathbf{u}] \rightarrow 0$ as we move away from the boundary, for $\varepsilon \rightarrow 0$. The value of $J_2[\mathbf{u}]$ tends to a constant as we move away from the boundary because of the quadratic term X_3^2 in $v_{b,3}^1$ as explained in Section 3.2.

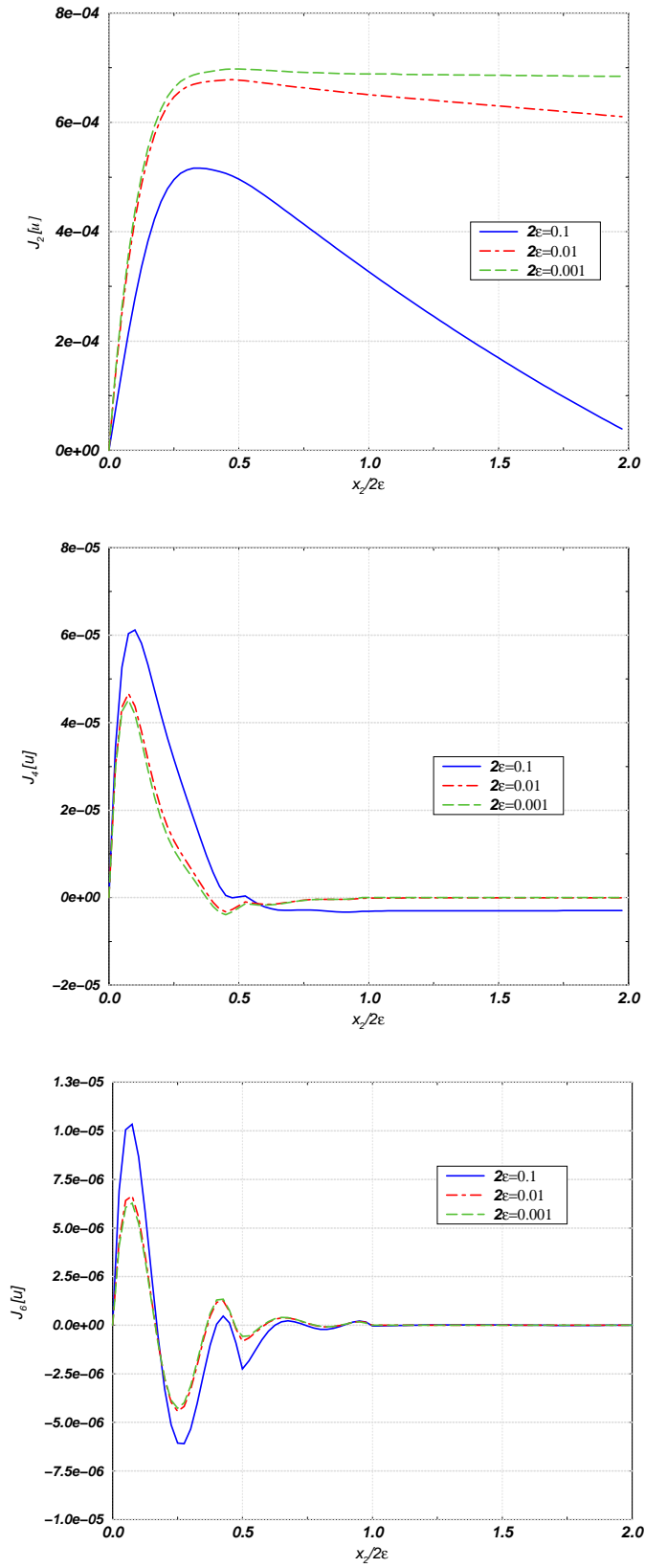


Figure 7: $J_2[u]$, $J_4[u]$ and $J_6[u]$ for straight boundary with ①

(ii) STRAINS IN THE BOUNDARY LAYER ZONE

The effect of the boundary layer is visible directly on the strain components $e_{b,s3} = e_{13}$ or $e_{b,n3} = e_{23}$ as $\varepsilon \rightarrow 0$, according to (3.15) for conditions ①–③, (3.17) for condition ④ and (3.18) for conditions ⑤–⑧.

In Figure 8 we plot $\log(I_{13}^{bl}) = \log(I_{s3}^{bl})$ (defined in (4.1)) vis $\log(2\varepsilon)$ for all boundary conditions ①–⑧ (\log herein denotes \log_{10}). One may clearly see the boundary layer

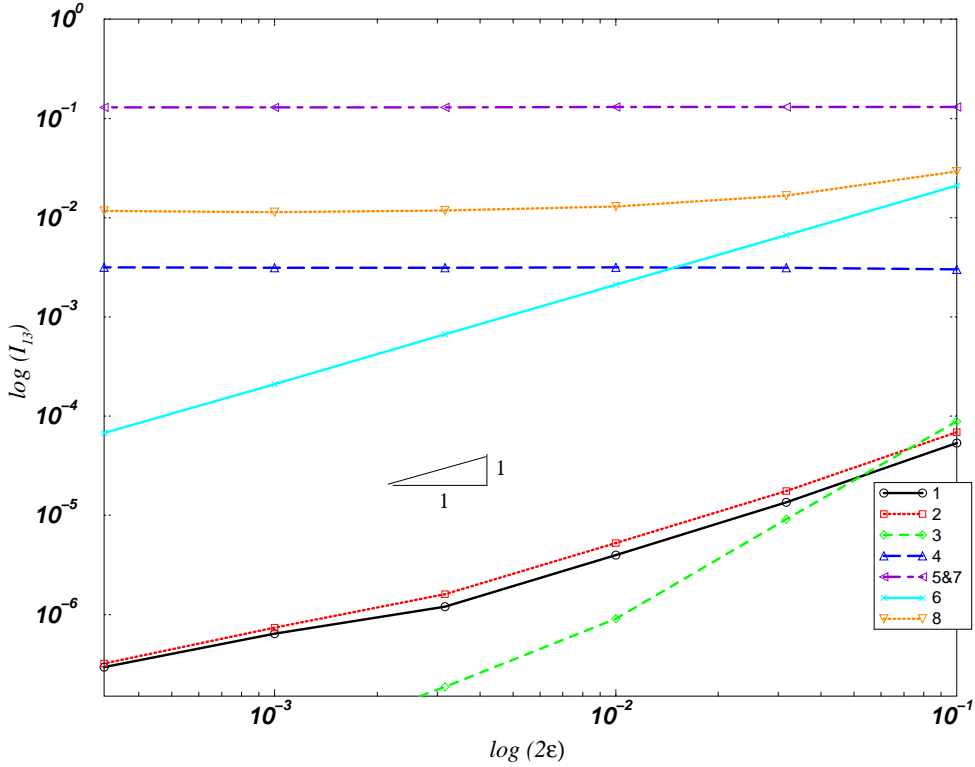


Figure 8: $\log(I_{13}^{bl}) = \log(I_{s3}^{bl})$ vis $\log(2\varepsilon)$ for ①–⑧ BCs (straight boundary).

effects for boundary conditions ④, ⑤, ⑦ and ⑧ which are manifested by the nearly constant value of $\log(I_{s3}^{bl})$ as $\varepsilon \rightarrow 0$, as predicted by the mathematical analysis. As predicted for straight boundaries, no boundary layer is visible for ③ and ⑥.

We plot in Figure 9 the values of $\log(I_{23}^{bl}) = \log(I_{n3}^{bl})$ as $\varepsilon \rightarrow 0$ for all boundary conditions ①–⑧. The value of $\log(I_{n3}^{bl})$ for ⑥ is virtually zero so that it is not shown in Figure 9. Again, the boundary layer effect is clearly visible for ① and ②: I_{n3}^{bl} approaches a constant value as $\varepsilon \rightarrow 0$. This is due to the $\mathcal{O}(1)$ component of the boundary layer profile, which may be smaller compared to $\frac{\varepsilon}{2}\partial_2 v_3^1$ for large values of ε , but much larger as $\varepsilon \rightarrow 0$.

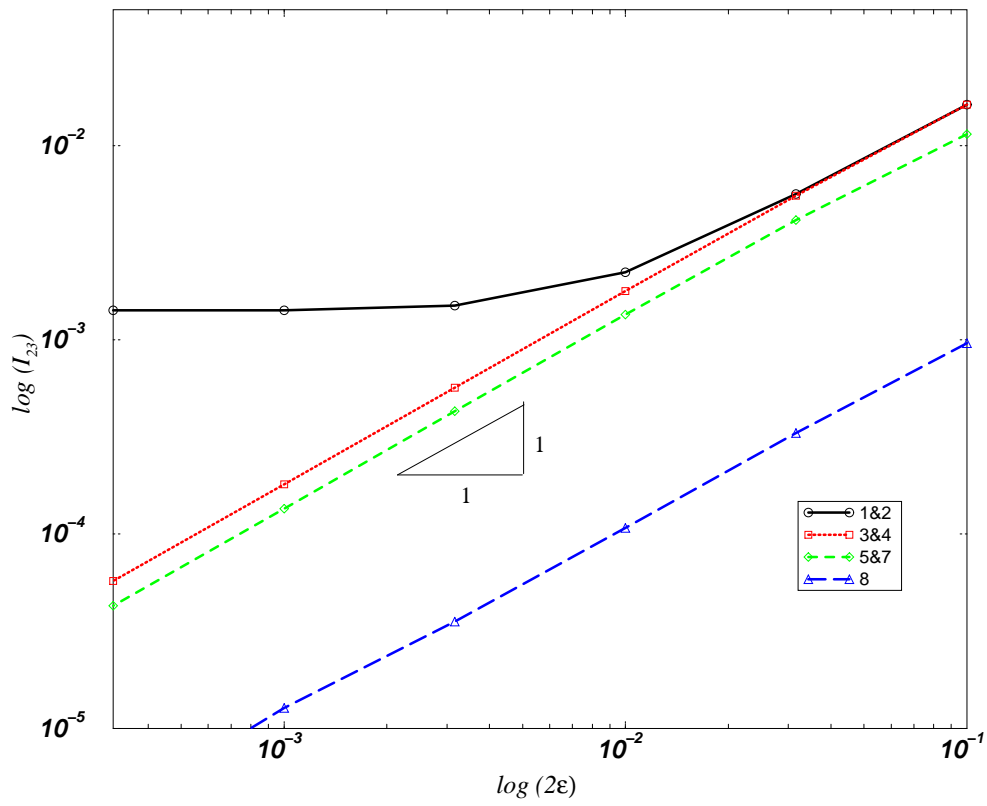


Figure 9: $\log(I_{23}^{bl}) = \log(I_{n3}^{bl})$ vis $\log(2\epsilon)$ for ① - ⑧ BCs (straight boundary).

(iii) STRAINS OUTSIDE THE BOUNDARY LAYER ZONE

For comparison purposes, we present the N-RMS norm computed outside of the boundary layer, defined in (4.2). This shows that, for all boundary conditions, both I_{13}^{out} and I_{23}^{out} are of order ε as the thickness tends to zero, due to the leading term of order ε in the strain components according to (3.10).

In Figure 10 we plot $\log(I_{13}^{out})$ vis $\log(2\varepsilon)$.

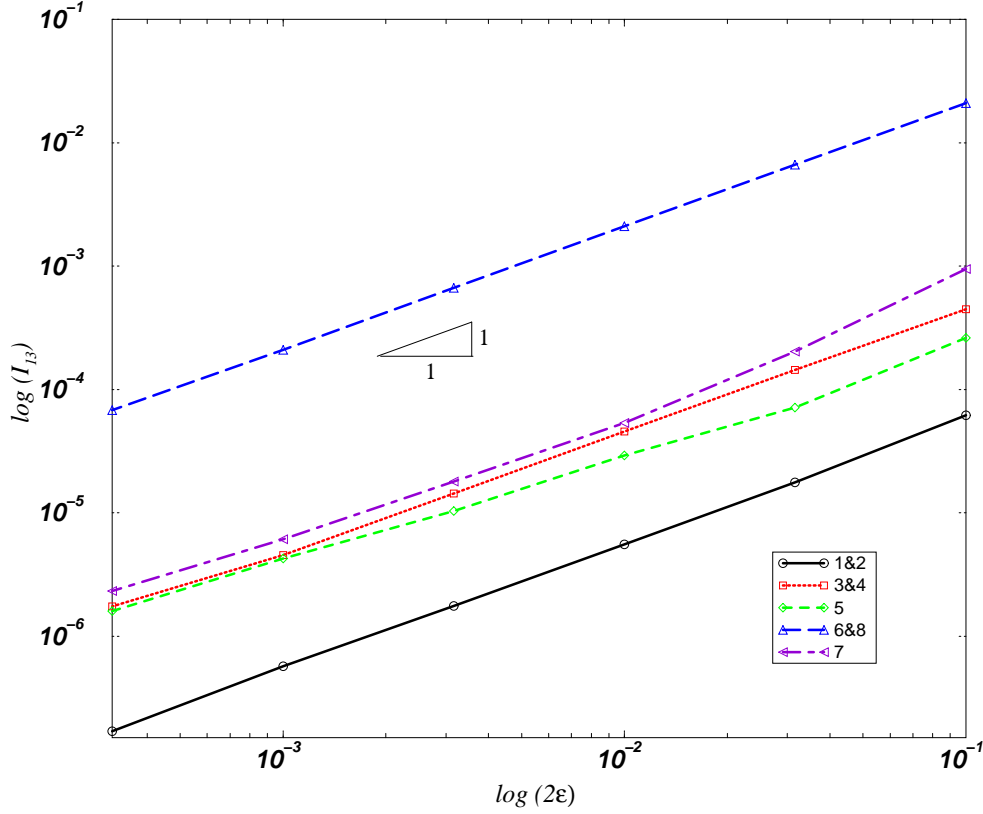


Figure 10: $\log(I_{13}^{out})$ vis $\log(2\varepsilon)$ for ① - ⑧ BCs (straight boundary).

In Figure 11 we plot $\log(I_{23}^{out})$ vis $\log(2\varepsilon)$. Because I_{23}^{out} is nearly zero for ⑥ boundary condition, it has not been shown in Figure 11.

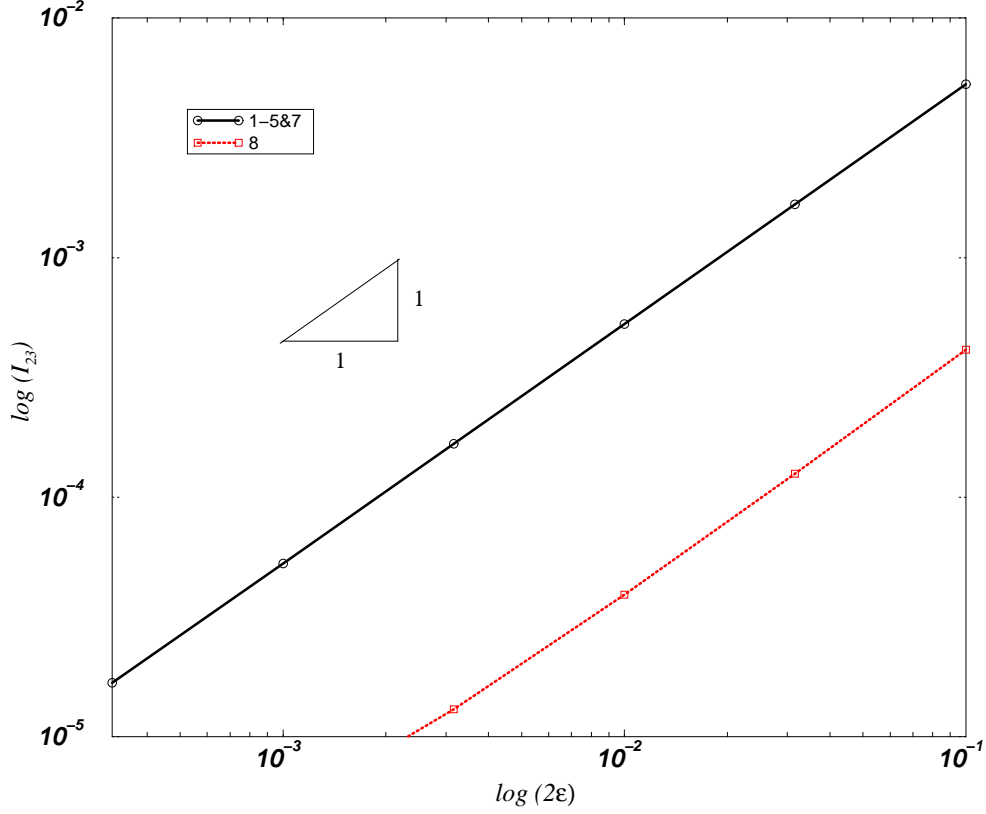


Figure 11: $\log(I_{23}^{out})$ vis $\log(2\varepsilon)$ for ① - ⑤ and ⑦ - ⑧ BCs (straight boundary).

5.2 Boundary layers in 3-D Soft Simply Supported ④ Circular Plate

Consider the plate shown in Figure 3, with soft simply supported boundary conditions $u_3 = 0$, $T_s = T_n = 0$, prescribed along the circular boundary.

Since the geometry, loading and boundary conditions are independent of θ , then we may analyze the plate as an axisymmetric model, having a two dimensional sector of radius 1 and thickness of 2ε . The finite element mesh used in our analysis is shown in Figure 12.

We consider the N-RMS norm of the strain component e_{n3} defined by (4.3) inside the boundary layer. In Figure 13 we plot $\log(I_{n3}^{bl})$ vis $\log(2\varepsilon)$. As expected, I_{n3}^{bl} is independent of ε , as $\varepsilon \rightarrow 0$ for curved boundaries, demonstrating a boundary layer profile as opposed to the case of a straight boundary. One may observe in (3.17) that e_{n3} for curved boundary is of order 1.

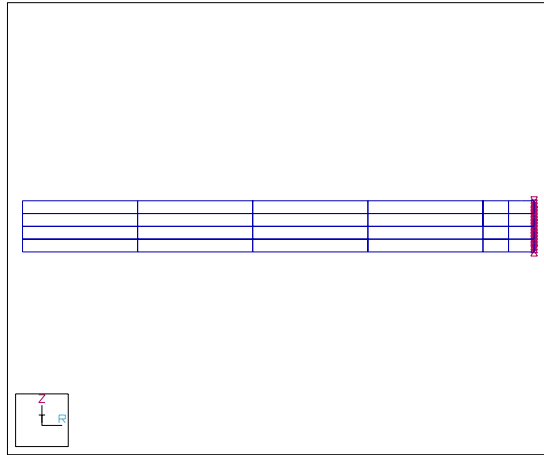


Figure 12: Finite element mesh and boundary conditions for the circular plate $2\varepsilon = 0.1$.

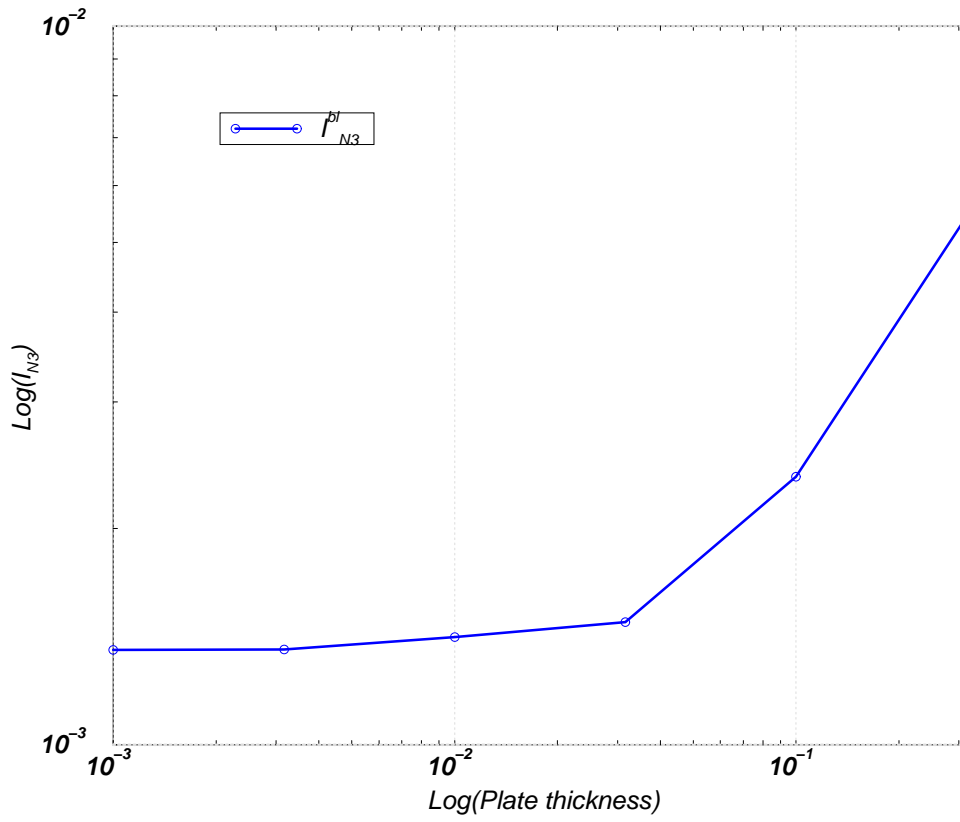


Figure 13: $\log(I_{n3}^{bl})$ vis $\log(2\varepsilon)$ for circular plate with ④

6 TWO-DIMENSIONAL FORMULATION OF HIERARCHIC PLATE-MODELS

Hierarchic plate-models have been formulated in the past ten years, and the reader is referred to [17, 8, 18, 14] for early references and [2, 3] for mixed hierarchical models using the Hellinger-Reissner principle.

Here follows a short overview on hierarchic plate models in the framework of the code that we use [1]: A hierarchical family of plate-models, denoted by the index d (for which its solution is defined as \mathbf{u}_d^ε) is one which satisfies:

- a) $\|\mathbf{u}^\varepsilon - \mathbf{u}_d^\varepsilon\|/\|\mathbf{u}^\varepsilon\| \rightarrow 0$, as $\varepsilon \rightarrow 0$. Usually the energy norm is used.
- b) If the solution \mathbf{u}^ε is sufficiently smooth with respect to ε then:

$$\|\mathbf{u}^\varepsilon - \mathbf{u}_d^\varepsilon\|/\|\mathbf{u}^\varepsilon\| \leq C(d) \varepsilon^{\alpha(d)}$$

with $\alpha(d) > \alpha(d-1)$.

- c) For any fixed ε

$$\|\mathbf{u}^\varepsilon - \mathbf{u}_d^\varepsilon\|/\|\mathbf{u}^\varepsilon\| \rightarrow 0, \quad \text{as } d \rightarrow \infty.$$

The displacements \mathbf{u}_d^ε of the plate-model d are:

$$\mathbf{u}_d^\varepsilon = \left\{ \begin{array}{l} \sum_{j=1}^{n_1} u_{1|j}(x_1, x_2) w_{1|j}(x_3) \\ \sum_{j=1}^{n_2} u_{2|j}(x_1, x_2) w_{2|j}(x_3) \\ \sum_{j=1}^{n_3} u_{3|j}(x_1, x_2) w_{3|j}(x_3) \end{array} \right\}. \quad (6.1)$$

Herein d is the number of the model, which coincides with the highest polynomial degree describing the displacement components. We will be considering the hierarchic plate-model family implemented in the finite element code Stress Check[†] [1], for which (note that this code aims at solving the bending equations whereas membrane, or stretching, models are variants of generalized plane-stress situations which are not addressed here):

Table 4: Hierarchic plate-model definitions.

d	(n_1, n_2, n_3)	Non-zero $w_1 = w_2$	Non-zero w_3
1	(1,1,1)	$w_{1 1} = w_{2 1} = x_3$	$w_{3 1} = 1$
2	(1,1,2)	$w_{1 1} = w_{2 1} = x_3$	$w_{3 1} = 1, w_{3 2} = x_3^2$
3	(2,2,2)	$w_{1 1} = w_{2 1} = x_3$ $w_{1 2} = w_{2 2} = x_3^3$	$w_{3 1} = 1, w_{3 2} = x_3^2$
4	(2,2,3)	$w_{1 1} = w_{2 1} = x_3$ $w_{1 2} = w_{2 2} = x_3^3$	$w_{3 1} = 1, w_{3 2} = x_3^2$ $w_{3 3} = x_3^4$
5	(3,3,3)	$w_{1 1} = w_{2 1} = x_3$ $w_{1 2} = w_{2 2} = x_3^3$ $w_{1 3} = w_{2 3} = x_3^5$	$w_{3 1} = 1, w_{3 2} = x_3^2$ $w_{3 3} = x_3^4$

[†] Stress Check is a trade mark of Engineering Software Research and Development, Inc., Clayton Plaza, Suite 204, 7750 Clayton rd., St. Louis, MO, USA

The first hierarchical plate-model $d = 1$ with the special material matrix given in [1, p.A11] is exactly the R-M model, where the shear correction factor is chosen so as to minimize the error in the energy norm:

$$\text{shear corr. factor} = \frac{5}{6(1 - \nu)}.$$

For $d = 2$ the shear correction factor is given in [1, p. 15.20-15.21] and for $d \geq 3$ no shear correction factor in the material matrix is needed.

Remark 6.1 *The K-L plate-model is not a member of the hierarchical family. It represents in a decoupled system the solution of the bending equation for ζ_3 :*

$$D\Delta_*^2 \zeta_3(x_1, x_2) = f_3(x_1, x_2), \quad D = \frac{E(2\varepsilon)^3}{12(1 - \nu)^2},$$

and a membrane equation for \mathbf{u}_* , and this solution is unable to manifest boundary layers.

7 NUMERICAL TESTS FOR COMPARING 3-D AND 2-D PLATE MODELS

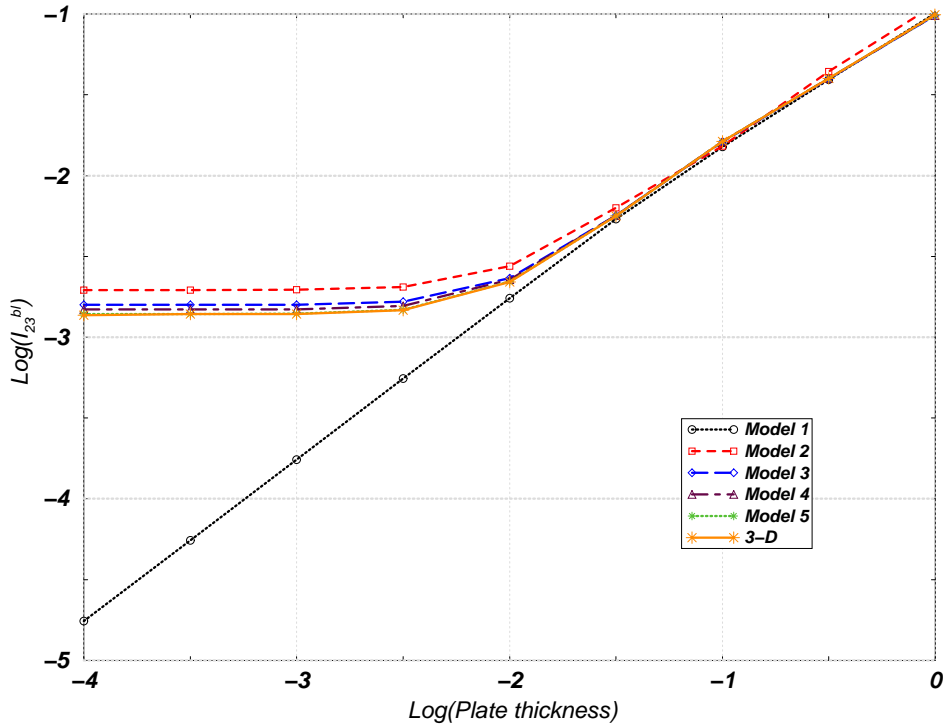


Figure 14: 3-D vis 2-D plate models: $\log(I_{23}^{bl})$ vis $\log(2\varepsilon)$ for ①

Of major interest is the question whether the various hierarchic plate models are able to capture the boundary layers present in 3-D domains. To address this question we consider the five hierarchic plate models having $d = 1, 2, 3, 4$ and 5 , and we denote them by model 1, 2, 3, 4 and 5 correspondingly. For the plate models, we consider the mid-surface of the

3-D domain, with a vertical pressure of a magnitude ε^2 applied on it. On the 2-D surface we lay a finite element mesh identical to the mesh on any plane (x_1, x_2) of the 3-D model presented in Figure 4. The first plate-model $d = 1$ with a special material matrix is the R-M model. For this R-M model, the hard clamped boundary conditions are applied by imposing zero displacements in all directions, which implies zero slope normal and tangential to the plate boundary. In all plate models the convergence rate in energy norm is exponential as well as the convergence rate of the strains.

Herein we analyze only three kinds of boundary conditions along a straight edge: ①, ⑥ and ⑧, and compare the plate model's boundary layer against the 3-D domain boundary layer.

7.1 Hard Clamped Plate ①

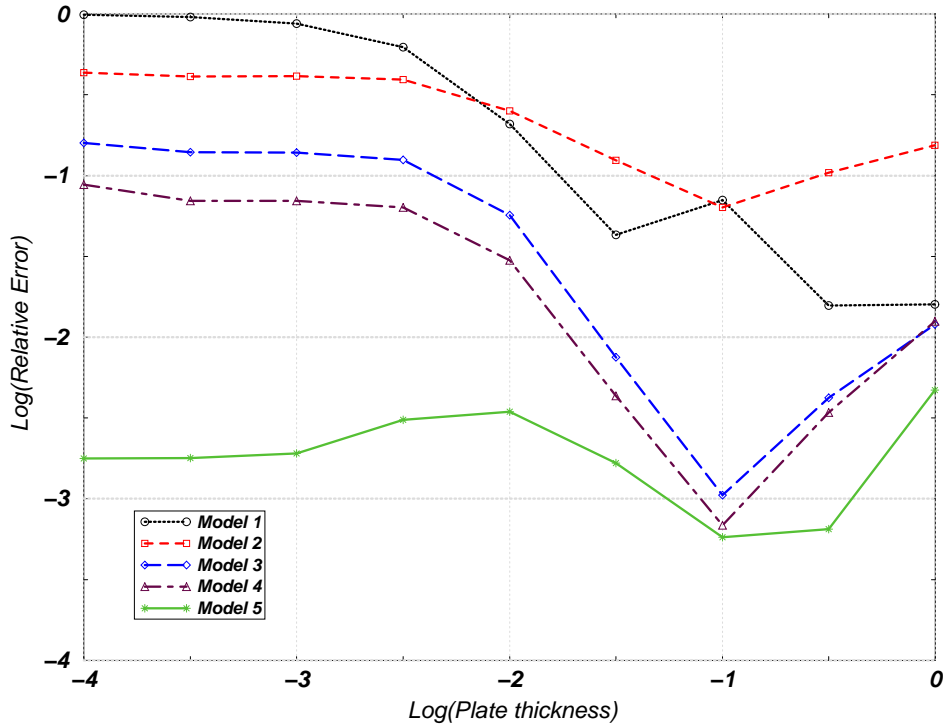


Figure 15: \log of rel. err. in I_{23}^{bl} between the 3-D and 2-D plate models as $\varepsilon \rightarrow 0$ for ①

The value of $\log(I_{23}^{bl})$ for the various 2-D plate models is plotted against the value obtained for the 3-D domain as $\varepsilon \rightarrow 0$ in Figure 14. One may notice that the R-M plate model (model 1) cannot mimic the boundary layer term. However, as we increase the order of hierarchic plate models a better approximation of the boundary layer is obtained. A more pronounced difference between the 3-D solution and the 2-D plate models is visible once we plot in Figure 15 the relative error in I_{23}^{bl} between the 3-D domain and the plate models:

$$\text{Relative Error} \stackrel{\text{def}}{=} \left| \frac{I_{23}^{bl}|_{3-D} - I_{23}^{bl}|_{2-D \text{ model}}}{I_{23}^{bl}|_{3-D}} \right|$$

as $\varepsilon \rightarrow 0$. Figure 15 shows how well the boundary layer term in the fully 3-D solution is represented by the various plate models as $\varepsilon \rightarrow 0$. It is also interesting to inspect the relative error in I_{23}^{bl} between the 3-D and 2-D plate models as the model number is increased, for the different thicknesses. This is shown in Figure 16. One may notice that

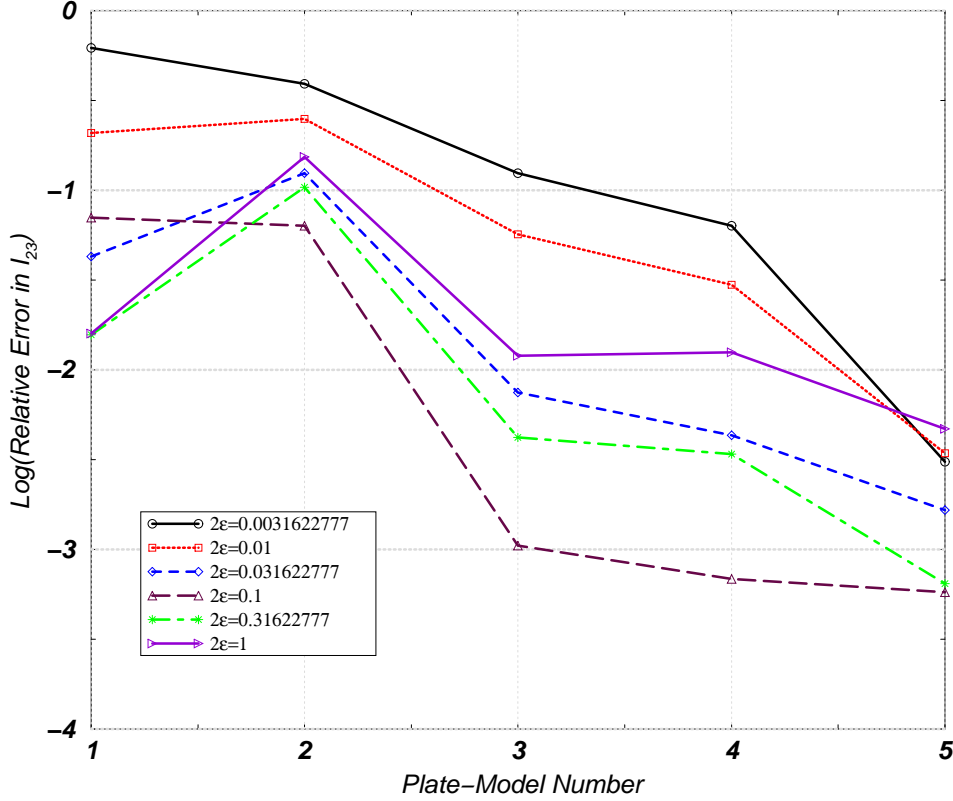


Figure 16: \log of rel. err. in I_{23}^{bl} between the 3-D and 2-D plate models as the model number is increased for (1)

plate model 2 does not always approximate better the boundary layer zone as compared to the R-M plate model. As the plate hierarchy increases, the better the approximability of boundary layers, independent of the thickness.

If one is interested in the outer field (away from the boundary layer zone), the relative error in I_{23}^{out} can be analyzed. In Figure 17 we plot the relative error in I_{23}^{out} between the 3-D model and the various plate models as $\varepsilon \rightarrow 0$. Away from the boundary layer a much smaller relative error is visible.

7.2 Comparing 3-D and 2-D Plate Models - Free Plate (8)

Herein we examine the value of $\log(I_{13}^{bl})$ associated with the boundary layer of the free boundary. It is plotted in Figure 18 for various 2-D plate models against the value obtained for the 3-D domain as $\varepsilon \rightarrow 0$. In this case, even the first plate model (R-M), is very close to the 3-D solution, capturing the boundary layer term well. Due to numerical errors in the

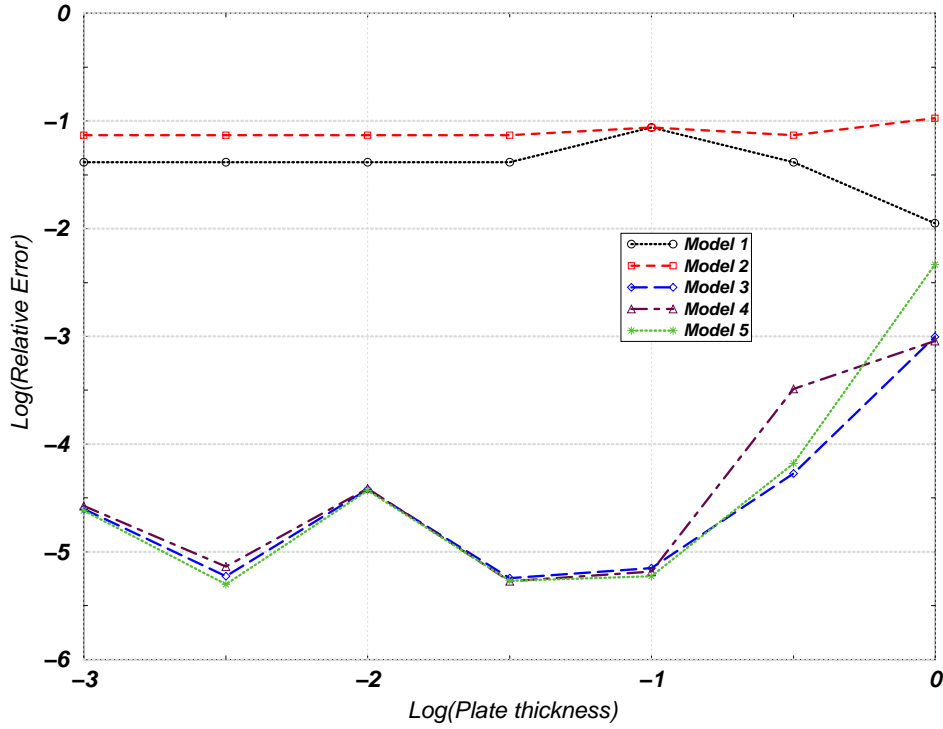


Figure 17: \log of relative error in I_{23}^{out} between the 3-D and 2-D plate models as $\varepsilon \rightarrow 0$ for ①

3-D models at $2\varepsilon < 10^{-3.5}$ we were not able to compute I_{13}^{bl} and I_{13}^{out} reliably, so that this value is extrapolated using previous two results in Figure 18 and 20 for the smallest two values of ε . In Figure 19 we inspect the relative error in I_{13}^{bl} between the 3-D and 2-D plate models as the model number is increased, for the different thicknesses. Again, one may notice that plate model 2 does not always approximate better the boundary layer zone as compared to the R-M plate model.

The value of I_{13}^{out} (away from the boundary layer zone) for the 3-D model and the various plate models as $\varepsilon \rightarrow 0$ is plotted in Figure 18. Again, one notices the very good agreement between the various plate models and the fully 3-D solution away from the boundary layer.

7.3 Comparing 3-D and 2-D Plate Models - Slide Plate ⑥

Herein we examine the value of $\log(I_{13}^{bl})$ associated with the boundary layer of the sliding boundary condition. As predicted, this value should approach zero as $\varepsilon \rightarrow 0$, since no boundary layer profile exists, therefore the same behavior is expected from the various 2-D plate models. Figure 21 shows $\log(I_{13}^{bl})$ for various 2-D plate models against the value obtained for the 3-D domain as $\varepsilon \rightarrow 0$. In this case, all plate models mimic the 3-D solution due to un-existence of boundary layers.

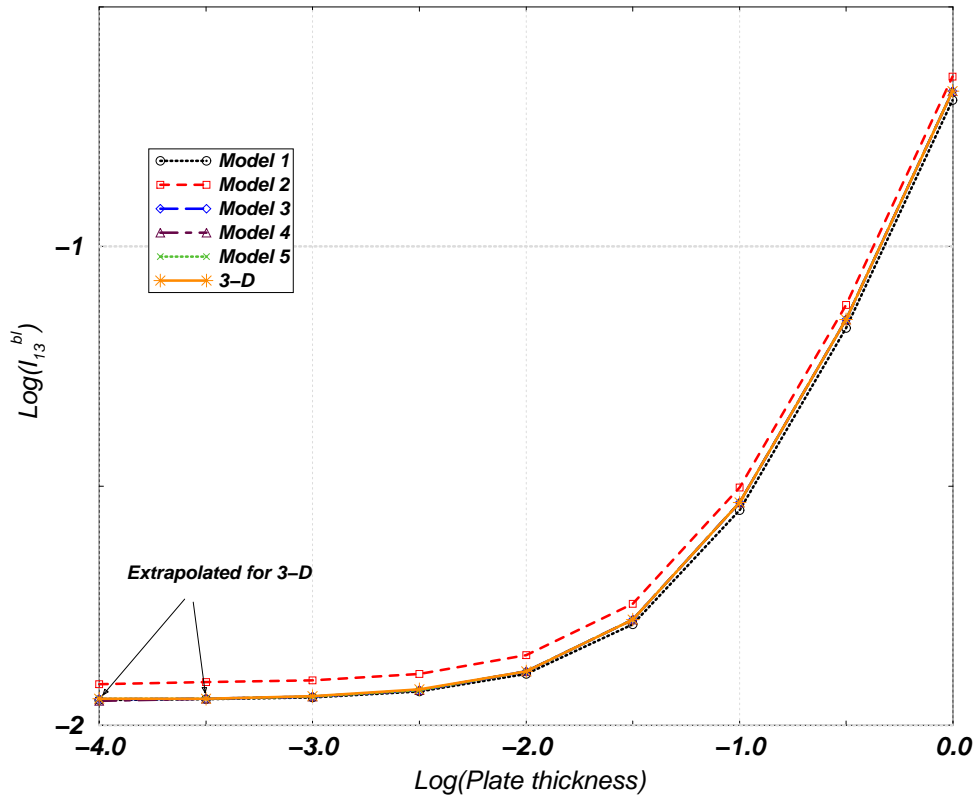


Figure 18: 3-D vis 2-D plate models: $\log(I_{13}^{bl})$ vis $\log(2\varepsilon)$ for $\textcircled{8}$

8 SUMMARY AND CONCLUSIONS

The solution of the elasticity problem in three-dimensional thin domains (having a thickness of 2ε) has been explicitly provided as an asymptotic series in ε . It has terms which exist in the boundary layer zone, which is of magnitude ε , and vanish away from it. This enables to identify, and more importantly quantify, the quantities which are rapidly changing in the boundary layer zone. Numerical experiments using the p-version of the finite element method, show that some of the strain components (thus the associated stress components) may be solely influenced by the boundary layer terms in the vicinity of boundary layers.

We also examine how well the various hierarchic plate models approximate the three-dimensional solution as $\varepsilon \rightarrow 0$. It has been demonstrated that for some boundary conditions, $\textcircled{8}$ for example, even the lowest member of the hierarchic plates family (R-M model) is able to capture the right boundary layer behavior, whereas for other boundary conditions, $\textcircled{1}$ for example, the R-M plate model completely misses its behavior for some of the strain components. When no boundary layers exist in the 3-D solution, $\textcircled{6}$ for example, then plate models mimic the 3-D solution in the “boundary layer” zone well. In all examined cases as we increase the hierarchic order of the plate models we converge to the right boundary layer representation.

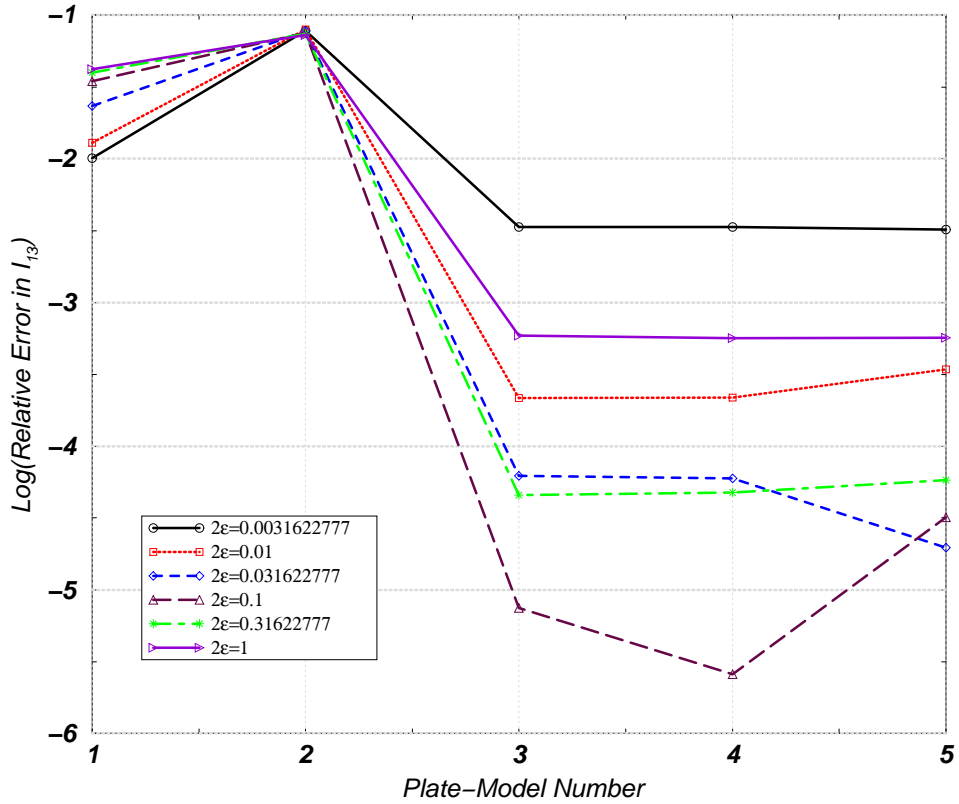


Figure 19: \log of rel. err. in I_{13}^{bl} between the 3-D and 2-D plate models as the model number is increased for (8)

The three-dimensional solution in the outer zone (away from the boundary layer) is much better approximated by the various plate models. It is important to note that all finite element models used have a proper mesh refinement towards the boundary layer zone. An improper mesh layout may cause numerical pollution errors from the boundary layer zone into the whole plate, thus even if the boundary layer solution is not of interest, a proper mesh layout is necessary to ensure control of numerical errors (see [16] for example).

There might be pathological cases in which the boundary layer terms will highly influence the solution away from the boundary, a subject which is under investigation.

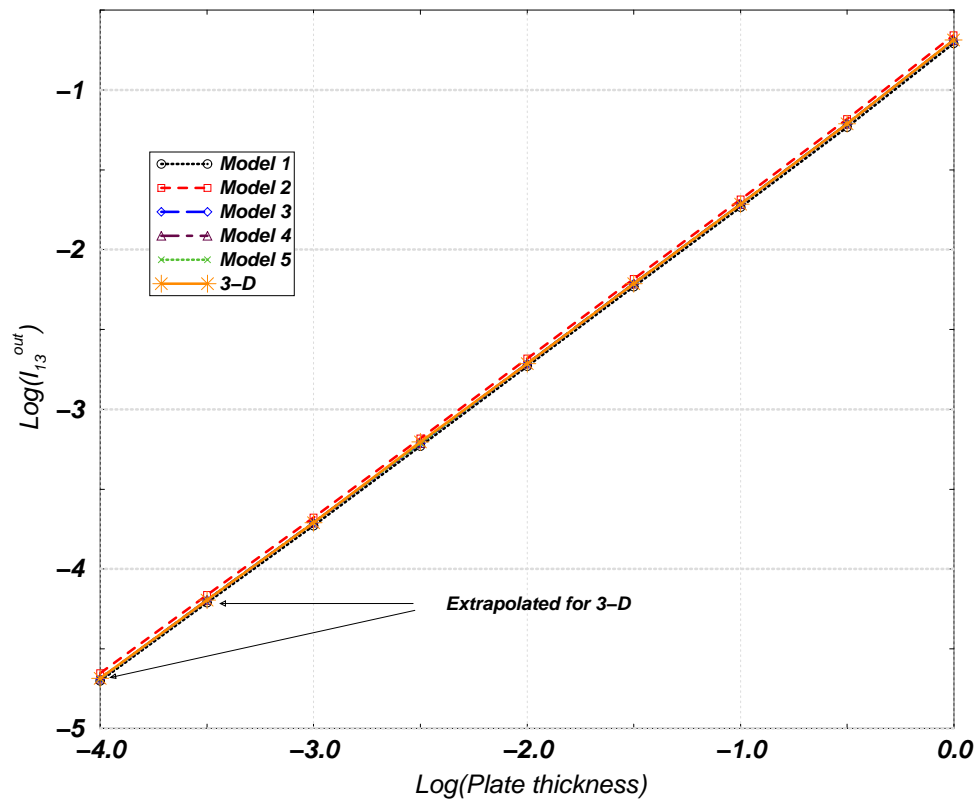


Figure 20: 3-D vis 2-D plate models: $\log(I_{13}^{out})$ vis $\log(2\varepsilon)$ for ⑧

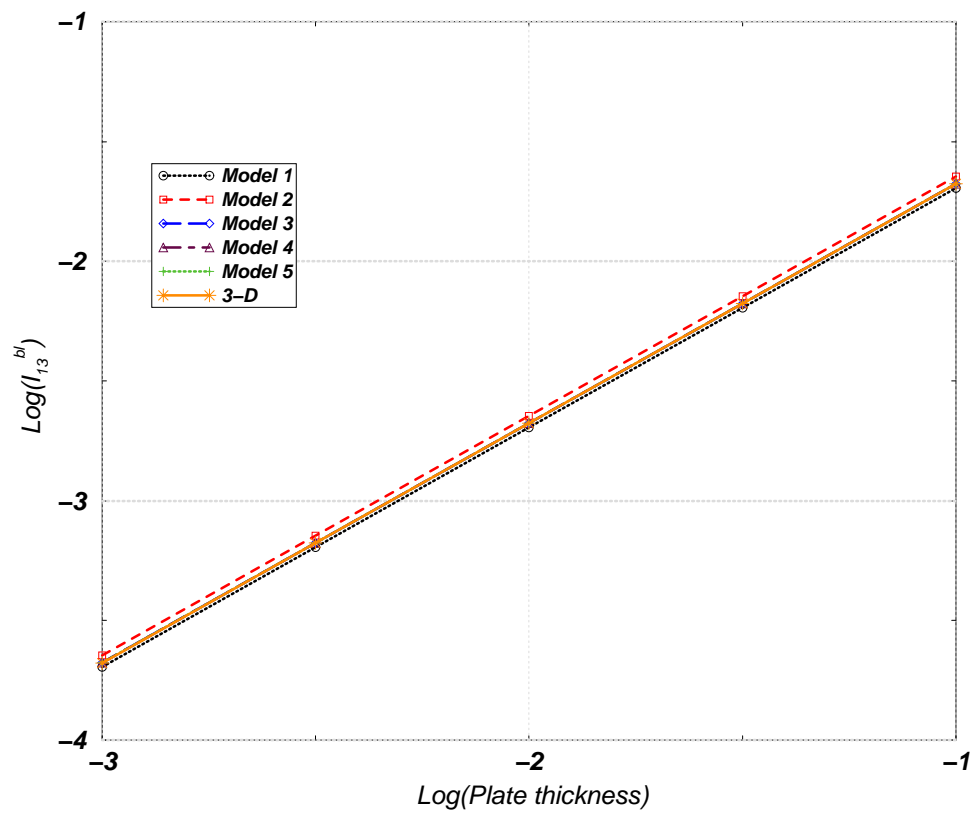


Figure 21: 3-D vis 2-D plate models: $\log(I_{13}^{bl})$ vis $\log(2\varepsilon)$ for ⑥

REFERENCES

- [1] *Stress Check User's Manual, Release 2.0*. ESRD, St. Louis, USA 1996.
- [2] S. M. ALESSANDRINI, D. N. ARNOLD, R. S. FALK, A. L. MADUREIRA. Derivation and justification of plate models by variational methods. In *Proceeding of the summer seminar of the Canadian Mathematical Society on "Plates and shells: from mathematical theory to engineering practice"*, CRM Proceeding and Lecture Notes. Quebec 1996.
- [3] S. M. ALESSANDRINI, D. N. ARNOLD, R. S. FALK, A. L. MADUREIRA. Dimensional reduction based on mixed variational principles. In M. BERNADOU, P. G. CIARLET, J. M. VIAÑO, editors, *Shells: mathematical modelling and scientific computing*, Cursos e congressos da Universidade de Santiago de Compostela, pages 25–28 1997.
- [4] D. ARNOLD, R. FALK. Edge effects in the Reissner-Mindlin plate model. In A. NOOR, T. BELYTSCHKO, J. SIMO, editors, *Analytical and Computational Models for Shells.*, pages 71–90. American Society of Mechanical Engineers, New York 1990.
- [5] D. N. ARNOLD, R. S. FALK. The boundary layer for the Reissner-Mindlin plate model. *SIAM J. Math. Anal.* **21** (2) (1990) 281–312.
- [6] D. N. ARNOLD, R. S. FALK. Asymptotic analysis of the boundary layer for the Reissner-Mindlin plate model. *SIAM J. Math. Anal.* **27** (2) (1996) 486–514.
- [7] I. BABUŠKA, L. LI. The problem of plate modelling: Theoretical and computational results. *Comput. Meth. Appl. Mech. Engrg.* **100** (1992) 249–273.
- [8] I. BABUŠKA, L. LI. Hierarchic modeling of plates. *Comput. & Structures* **40** (1991) 419–430.
- [9] I. BABUŠKA, L. LI. The h-p-version of the finite element method in the plate modelling problem. *Comm. Appl. Numer. Meth.* **8** (1992) 17–26.
- [10] P. G. CIARLET. *Plates and Junctions in Elastic Multi-Structures: An Asymptotic Analysis*. R.M.A. Vol. 14. Masson and Springer-Verlag, Paris and Heidelberg 1990.
- [11] M. DAUGE, I. GRUAIS, A. RÖSSLE. The influence of lateral boundary conditions on the asymptotics in thin elastic plates I & II. Prépublications 97-28 & 97-29, IRMAR 1997. On the web: <http://www.maths.univ-rennes1.fr/~dauge/> .
- [12] M. DAUGE, I. GRUAIS, A. RÖSSLE. The influence of lateral boundary conditions on the asymptotics in thin elastic plates. *Submitted to SIAM Jour. of Math. Anal.* (1998).
- [13] K. O. FRIEDRICHS, R. F. DRESSLER. A boundary-layer theory for elastic plates. *Comm. Pure Appl. Math.* **14** (1961) 1–33.
- [14] C. SCHWAB. The dimension reduction method. Ph. d. thesis, University of Maryland, College Park. 1989.
- [15] C. SCHWAB, M. SURI. The p and hp versions of the finite element method for problems with boundary layers. *Math. Comp.* **65** (1996) 1403–1429.
- [16] M. SURI, C. SCHWAB, C. XENOPHONTOS. The hp finite element method for problems in mechanics with boundary layers. *Comp. Meth. Appl. Mech. Engrg.* **157** (1998) 311–333.
- [17] B. SZABÓ, I. BABUŠKA. *Finite Element Analysis*. Willey, New-York 1991.
- [18] B. SZABÓ, G. SAHRMANN. Hierarchic plate and shell models based on p-extension. *Int. Jour. Numer. Meth. Engrg.* **26** (1988) 1855–1881.